Online Resource 2 for the manuscript: In-situ measurement of the large strain response of the fibrillar debonding region during the steady peeling of Pressure Sensitive Adhesives

Richard Villey,[a,b], Pierre-Philippe Cortet,[b] Costantino Creton,[a] and Matteo Ciccotti,[a]

Work of cohesive forces during peeling (demonstration of Eq. 12)

To calculate the work of the cohesive forces corresponding to a small advance by dc of the peeling front (corresponding in our model to the clamping position of the tape backing), let us consider the local displacement of the tape backing from point M (see Fig. S1), of coordinates $[x(s), y(s)]$ in the initial frame of reference $(O, \vec{e}_x, \vec{e}_y)$, to point M' of coordinates $[x(s+dc), y(s+dc)]$ in the translated frame of reference $(O', \vec{e}_x, \vec{e}_y)$:

$$\overrightarrow{MM'} = \overrightarrow{MO} + \overrightarrow{OO'} + \overrightarrow{O'M'} = \begin{pmatrix} -x(s) \\ -y(s) \end{pmatrix} + \begin{pmatrix} -dc \\ 0 \end{pmatrix} + \begin{pmatrix} x(s+dc) \\ y(s+dc) \end{pmatrix}, \tag{S1}$$

which gives for $dc \to 0$:

$$\frac{\overrightarrow{dM}}{dc} = \begin{pmatrix} \cos\alpha - 1 \\ \sin\alpha \end{pmatrix}. \tag{S2}$$

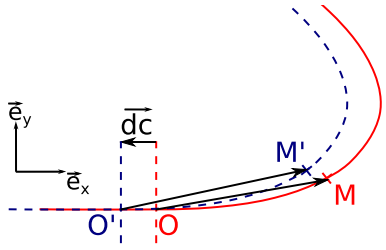

Fig. S1 Displacement of the tape backing during a fracture advance by dc.

Multiplying $\overrightarrow{dM}$ by the local cohesive force $\overrightarrow{dR} = \bar{\sigma} b ds \left[-\cos(\varphi)\overrightarrow{e_x} + \sin(\varphi)\overrightarrow{e_y}\right]$ and integrating over the cohesive zone gives the work $dW_{\bar{\sigma}}$ of the cohesive forces associated to the fracture advance dc:

$$dW_{\bar{\sigma}} = \int_{s=0}^{l_s} \bar{\sigma} b ds \begin{pmatrix} -\cos\varphi \\ \sin\varphi \end{pmatrix} \cdot \begin{pmatrix} \cos\alpha - 1 \\ \sin\alpha \end{pmatrix} dc = \bar{\sigma} b dc \int_{s=0}^{l_s} \left[\frac{s-x}{a}(1-\cos\alpha) + \frac{a_0+y}{a}\sin\alpha \right] ds, \tag{S3}$$

where $a(s) = \sqrt{(s-x)^2 + (a_0+y)^2}$ is the length of the fibril attached on the tape backing at curvilinear abscissa s (see Fig. 4). During steady-state peeling, the work per unit area of fracture advance $dW_{\bar{\sigma}}/(bdc)$ used to stretch the fibrils should be equal to the work per unit area of the operator G (we neglect the elastic stretching of the tape backing as in Eq. 1), which implies:

$$G = \frac{dW_{\bar{\sigma}}}{bdc} = \bar{\sigma} \int_{s=0}^{l_s} \left[\frac{s-x}{a}\frac{d(s-x)}{ds} + \frac{a_0+y}{a}\frac{dy}{ds} \right] ds = \bar{\sigma} \int_{s=0}^{l_s} \frac{da(s)}{ds} ds = \bar{\sigma}\left(a_f - a_0\right), \tag{S4}$$

which is Eq. 12.

[a] *Laboratoire SIMM, UMR7615 ESPCI-CNRS-UPMC-PSL, France. E-mail: matteo.ciccotti@espci.fr*
[b] *Laboratoire FAST, CNRS, Univ. Paris-Sud, Université Paris-Saclay, France.*

An elastica model with a cohesive zone: approximated solutions

This section gives (semi-)analytical solutions to the system composed of linearised Eq. 7 and of boundary conditions Eqs. 10 and 11 (equivalent to linearised Eq. 14 and boundary conditions Eq. 13). These simplified solutions provide first guesses necessary to solve the exact numerical system, where no linearisation is performed.

The classical small angles approximations $\sin\alpha \approx \tan\alpha \approx \alpha \approx dy/dx$, $\cos\alpha \approx 1$ and $s \approx x$ (meaning the $'$ symbol refers to the derivative with respect to x in this section) imply in particular that $\varphi \approx \frac{\pi}{2}$ (fibrils are vertical). Using these simplifications and neglecting second-order or higher terms in y', Eq. 7 becomes:

$$r^2 y''' + \sin\theta - y'\cos\theta + \frac{x - l_x}{l_0} = 0 \quad \text{with} \quad l_0 = \frac{F}{\bar{\sigma} b}. \tag{S5}$$

Eq. S5 is a simple linear ordinary differential equation of the second order in y', the solution of which is:

$$y' = A e^{\frac{x\sqrt{\cos\theta}}{r}} + B e^{-\frac{x\sqrt{\cos\theta}}{r}} + \frac{x - l_x}{l_0 \cos\theta} + \tan\theta, \tag{S6}$$

with the boundary conditions

$$\begin{aligned} y'(0) &= 0, \\ y''(0) &= 0, \\ y'(l_x) &= \theta - 4\arctan X, \\ y''(l_x) &= \frac{4X}{r\left(1 + X^2\right)} = \frac{2}{r}\sin\left(2\arctan X\right). \end{aligned} \tag{S7}$$

If $\theta \geq 90^{\text{o}}$ expression S6 can still be used, with its limit expression when $\theta \to 90^{\text{o}}$ (no divergence) or with imaginary exponential arguments at $\theta > 90^{\text{o}}$. Notice that $\arctan X$ cannot be linearised, since $y'(l_x)$ is supposed to be small, but not necessarily $\theta - y'(l_x)$.

To find A, B, l_0 (thus the average stress $\bar{\sigma}$) and X, we need to solve the system :

$$\begin{aligned} \mathbf{A} &= \frac{l_x}{2\mathbf{l_0}\cos\theta} - \frac{\tan\theta}{2} - \frac{r}{2\mathbf{l_0}(\cos\theta)^{\mathbf{3/2}}}, \\ \mathbf{B} &= \frac{l_x}{2\mathbf{l_0}\cos\theta} - \frac{\tan\theta}{2} + \frac{r}{2\mathbf{l_0}(\cos\theta)^{\mathbf{3/2}}}, \\ \mathbf{X} &= \tan\left(\frac{\theta - \tan\theta - \mathbf{A}\mathbf{e}^{\frac{\mathbf{l_x}\sqrt{\cos\theta}}{\mathbf{r}}} - \mathbf{B}\mathbf{e}^{-\frac{\mathbf{l_x}\sqrt{\cos\theta}}{\mathbf{r}}}}{4}\right), \\ &\frac{r}{2\mathbf{l_0}\cos\theta}\left\{\left[1 - \cosh\left(\frac{l_x\sqrt{\cos\theta}}{r}\right)\right] + \frac{l_x\sqrt{\cos\theta}}{r}\sinh\left(\frac{l_x\sqrt{\cos\theta}}{r}\right)\right\} - \frac{\sin\theta}{2\sqrt{\cos\theta}}\sinh\left(\frac{l_x\sqrt{\cos\theta}}{r}\right) \\ &= \sin\left\{\frac{r}{2\mathbf{l_0}\left(\cos\theta\right)^{\mathbf{3/2}}}\left[\sinh\left(\frac{l_x\sqrt{\cos\theta}}{r}\right) - \frac{l_x\sqrt{\cos\theta}}{r}\cosh\left(\frac{l_x\sqrt{\cos\theta}}{r}\right)\right] + \frac{\theta}{2} + \frac{\tan\theta}{2}\left[\cosh\left(\frac{l_x\sqrt{\cos\theta}}{r}\right) - 1\right]\right\}. \end{aligned} \tag{S8}$$

The last equation of this system (still valid at $\theta = 90^{\text{o}}$ if Taylor series in $\frac{l_x\sqrt{\cos\theta}}{r}$ are taken) is of type

$$a\frac{r}{l_0} + b = \sin\left(c\frac{r}{l_0} + d\right),$$

the solution of which is easy to find numerically, without the need for minimizing N lines like in the non-linearised system. Moreover, a sufficient condition for this solution to be unique is $|a| \geq |c|$ *i.e.*

$$\left|\sqrt{\cos\theta}\left[1 - \cosh(t) + t\sinh(t)\right]\right| \geq \left|\sinh(t) - t\cosh(t)\right| \quad \text{with} \quad t = \frac{l_x\sqrt{\cos\theta}}{r},$$

t being real or imaginary. This inequality is always verified if $l_x \leq r$; otherwise, it is only verified as long as θ is small enough. Both conditions correspond in fact to $\alpha(l_s)$ (or $y'(l_x)$) small enough, the assumption made in this simplified model. Actually, numerical simulations show that Eq. S8 can have a unique solution even when the inequality above is not respected (for example at $l_s = 3r$ the inequality is only verified for $\theta < 24.3^o$, but Eq. S8 still gives a solution not too far from that of the non-linearized system at $\theta = 60^o$, see Fig. S2).

Eqs. 9, S8 and S6 then enable to plot the whole $\alpha(s)$ (or $y(x)$ after integration) profile, inside and outside of the cohesive zone, providing a semi-analytical first guess to solve Eq. 14, the only non-analytic formula being the solution of $a\frac{r}{l_0} + b = \sin\left(c\frac{r}{l_0} + d\right)$.

A fully analytical solution is accessible if the angles are small inside and outside of the cohesive zone (*i.e.* θ is small). Using $\theta \approx \tan\theta \approx \sin\theta$ and $\cos\theta \approx 1$ in Eq. S6 and linearising the boundary conditions Eq. S7, we obtain :

$$
\begin{aligned}
y'(x \leq l_x) &= \theta\left[1 + \frac{\frac{x-l_x}{r} - \frac{1}{2}e^{\frac{x-l_x}{r}} + e^{\frac{-x}{r}}\left(1 - \frac{1}{2}e^{\frac{-l_x}{r}}\right)}{\frac{l_x}{r} + e^{\frac{-l_x}{r}} - 1}\right], \\
y'(x \geq l_x) &= \theta\left[1 + \frac{1 - \cosh\left(\frac{l_x}{r}\right)}{\frac{l_x}{r} + e^{\frac{-l_x}{r}} - 1}e^{\frac{-x}{r}}\right], \qquad \text{(S9)} \\
\text{with} \\
l_0 &= \frac{r}{\theta}\left(\frac{l_x}{r} + e^{\frac{-l_x}{r}} - 1\right) \quad \textit{i.e.} \quad \sigma = \frac{F\theta}{rb}\frac{1}{\frac{l_x}{r} + e^{\frac{-l_x}{r}} - 1}.
\end{aligned}
$$

This analytical solution is represented in Fig. S2, as well as the "semi-analytical" solution obtained in the limits of small angles in the cohesive zone (solution of Eqs. S6 and S8) and the exact numerical solutions (solution of Eqs. 13 and 14). Even for very large peeling angles θ, only small differences between the approximated and full numerical solutions are observed, as long as $l_s \leq r$. But when both l_s/r and θ become large enough, the approximated solutions depart from the numerical one. Surprisingly, the fully analytical solution seems to generally remain closer to the fully numerical solution than the semi-analytical one does, even though the former corresponds to more severe assumptions (all angles are small) than the latter (angles are small only in the cohesive zone).

These approximated solutions, and especially the fully analytical one, are therefore very useful first guesses for solving the full numerical system. However, the latter is still necessary to correctly fit experimental profiles, since even for close $\alpha(s)$ profiles, large differences can be observed in the $y(x)$ profiles (errors are cumulated by integration), and therefore on a_f, yielding possibly large differences for the average stress $\bar{\sigma} = \Gamma/(a_f - a_0)$ deduced from such a fit.

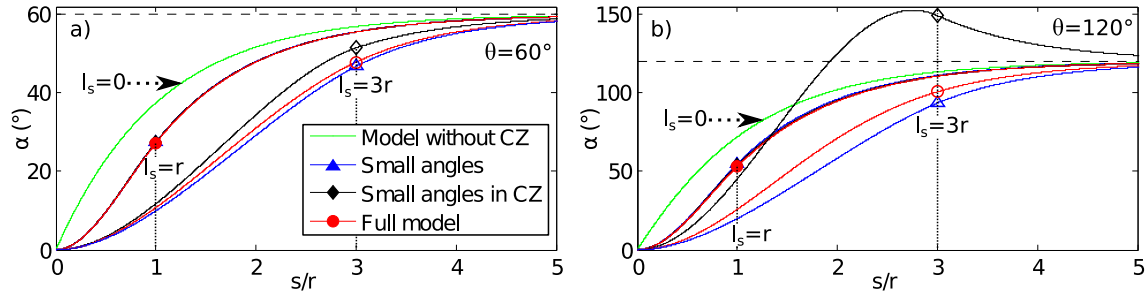

Fig. S2 Theoretical profiles of an elastica with cohesive zones (CZ) of different sizes l_s (in curvilinear abscissa) and at different peeling angles θ. The model with no cohesive zone ($l_s = 0$) corresponds to Eq. 4; the model at small angles corresponds to Eq. S9; the model at small angles in the cohesive zone corresponds to the numerical solution of system S8 injected in Eq. S6; the full numerical solution is obtained by solving the system composed of the boundary conditions Eqs. 13 and 14, using the small angles model as an initial guess. At l_s/r and/or θ small enough (*e.g.* here at $l_s = r$), these three models give almost undistinguishable $\alpha(s)$ profiles.